SEPTEMBER 1980 PPPL-1695

UC-20f

NEUTRONICS CALCULATIONS FOR THE TFTR NEUTRON CALORIMETER

BY

G. R. IMEL

PLASMA PHYSICS LABORATORY

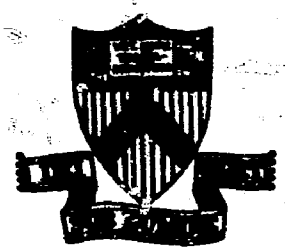

PRINCETON UNIVERSITY
PRINCETON, NEW JERSEY

This work was supported by the U.S. Department of Energy Contract No. DE-AC02-76-CHO 3073. Reproduction, translation, publication, use and disposal, in whole or in part, by or for the United States government is permitted.

NEUTRONICS CALCULATIONS FOR THE TFTR NEUTRON CALORIMETER

G. R. IMEL*

Plasma Physics Laboratory, Princeton University

Princeton, New Jersey 08544

ABSTRACT

Neutronics analyses have been performed for an adiabatic "neutron calorimeter" consisting of a pure hydrocarbon moderator located just outside of the vacuum vessel of the Tokamak Fusion Test Reactor. One and two-dimensional neutronic analyses show that the incident fusion neutron fluence can be determined to ± 10% uncertainty by simply integrating measured temperature profiles along the central radial axis (and assuming negligible error in the temperature measurement). The ± 10% uncertainty is found to be due to gamma rays produced by inelastic scattering and exothermic capture reactions in the moderator and vacuum vessel. The perturbing effects due to the toroidal field coils and due to gamma rays entering the sides of the calorimeter are shown to be negligible in the region of the central axis.

* On leave from EG&G, Idaho, Inc., Idaho Falls, ID 83415

I. INTRODUCTION

A "calorimeter" has been proposed as a fusion energy diagnostic for the Tokamak Fusion Test Reactor (TFTR).[1,2,3] Conceptually, the device consists of a neutron moderating material placed flush against the TFTR vacuum vessel. Temperature rise in the moderating medium will reflect the amount of energy absorbed from the slowing down of neutrons, which can be related to the incident neutron fluence, and ultimately to the fusion neutron source.

The selection of the moderator will be based on basic properties such as the elastic scatter cross-section (high), heat capacity (low), and heat conduction (low). These requirements imply a low density hydrogenous material; in fact, free hydrogen (such as liquid H_2) would probably be ideal. However, other aspects such as cost, safety, and ease of fabrication and operation must be considered. From such considerations, it appears that a pure hydrocarbon will be the most suitable material.[3] For the purpose of these initial neutronics calculations, a hydrogen-to-carbon atom ratio of 2:1 with a density of 0.6 g/cm^3 is used. This ratio describes the polyethelene molecule (CH_2), although at a much lower density, making these calculations conservative regarding neutron slowing down lengths (if polyethelene is indeed used as the moderating material).

The principal purpose of the neutronics calculations is to determine to what extent measured temperature increases can be related "absolutely" to the fusion neutron fluence incident on the calorimeter, and thence to the fusion neutron source. The following neutronics calculations will have to be redone when the final choice is made for the moderator and structural materials. However, these initial calculations do provide some measure of performance of the concept by showing approximate power deposition profiles (which can be related to measured temperature profiles), the effects of non-elastic gamma-

ray producing collisions, the effects of components such as TF coils, and the degree of isolation of the central axis from such effects. This report deals only with neutronics calculations in support of the calorimeter; other aspects such as methods for accurately measuring small temperature changes are discussed in Reference 3. (Summaries of References 2 and 3 are included in Appendix A of this report.)

II. MATERIAL COMPOSITIONS AND CROSS-SECTIONS

A 34 group cross-section set (23 neutron, 11 gamma) collapsed from DLC-37/EPR-D (available from the Reactor Shielding Information Center, RSIC, at Oak Ridge) was used for the following calculations. The 34 group structure is shown in Table 1. The mixing of the cross-sections to produce macroscopic cross-sections for the materials of interest was done using the component atomic number densities given in Table 2.

III. ONE DIMENSIONAL CALCULATIONS

The neutron transport code ANISN-PPL (available from RSIC) was used for one-dimensional calculations. The geometric model, an infinite cylinder with rotational symmetry, is shown in Figure 1. The isotropic source density of 2.4×10^{11} n/cm^3-sec in a 75 cm radius represents a total neutron production of 3.5×10^{18} 14 MeV neutrons per 0.5 second pulse of the TFTR plasma. The results described below can be scaled linearly to any neutron production in the TFTR. A listing of the ANISN input is given in Appendix B.

TABLE 1

34 GROUP STRUCTURE

Group	Neutron Energy Range (MeV)		
1	13.499	to	14.918
2	12.214		13.499
3	11.052		12.214
4	10.000		11.052
5	9.0484		10.000
6	7.4082		9.0484
7	6.0653		7.4082
8	4.9659		6.0653
9	4.0657		4.9659
10	3.3287		4.0657
11	2.7253		3.3287
12	2.2313		2.7253
13	1.8268		2.2313
14	1.0026		1.8268
15	5.5023-1		1.0026+0
16	2.0242-1		5.5023-1
17	4.0868-2		2.0242-1
18	3.3546-3		4.0868-2
19	2.7537-4		3.3546-3
20	2.2603-5		2.7537-4
21	1.8554-6		2.2603-5
22	4.1400-7		1.8554-6
23	THERMAL		
Group	Photon Energy Range (MeV)		
24	12	to	14
25	8		12
26	7		8
27	6		7
28	5		6
29	4		5
30	3		4
31	2		3
32	1		2
33	0.2		1
34	<0.2		

TABLE 2

MATERIAL COMPOSITIONS

Mixture	Nuclide	Atom Density ($x10^{24}$ cm^{-3})
SS-304	Ni	.0068
(vacuum vessel)	Cr	.017
	Fe	.061
	Mn-55	.0012
Air	N	.00004
	O	.000011
Vacuum	--	0
Nitronic - 33	Ni	.0024
(coil case)	Cr	.016
	Fe	.054
	Mn-55	.011
	Si	.0017
TF Coil	H	.0044
(homogenized)	O	.0050
	Cu	.072
	B-10	.000069
	B-11	.00027
	Si	.0012
	Ca	.00042
	Al	.00023
Igloo Concrete	H	.0082
	B-10	.00022
	B-11	.00088
	C	.011
	O	.043
	Na	.000013
	Mg	.00019
	Al	.00026
	Si	.0011
	S-32	.000081
	K	.000014
	Ca	.013
	Fe	.00015
	Ba	.00012
Lead (shield)	Pb	.033
Polyethelene	H	.054
	C	.027

For the neutron calorimeter, the parameter of interest is the spatial energy (or power) deposition. To determine the energy deposition for a given neutron spectrum (output from ANISN), so-called kerma factors (available in DLC-37) are used to calculate reaction rates (in this case, energy deposition rates). Radial power deposition profiles from 14 MeV neutrons (source neutrons), all other neutrons (fast neutrons) and gammas calculated using the model described above are shown in Figure 2. At the front face, the contribution from the source neutrons is about 50% of the total energy deposition (which is about 9×10^4 rads/second, or 4.5×10^4 rads/0.5 second pulse); the contribution from the fast neutrons is about 35% and from the gammas about 15%. At the back of the calorimeter the source component contributes only 5% to the total (which is about 2×10^3 rads/second or 1×10^3 rads/0.5 second pulse), the fast neutrons 20%, and the gammas 75%. However, the total energy deposition is down by almost two orders of magnitude at this point, so that the large percentage contribution by the gammas is of no practical importance. The total energy deposition is down by an order of magnitude at about 160 cm from the plasma centerline, or about 40 cm into the calorimeter. This point will subsequently be called the "decade point". At this point, the relative contributions are: 15% source neutrons, 50% fast neutrons, and 35% gammas.

It is seen by examining Figure 2 that temperature rise in the calorimeter will not be due solely to the direct slowing down of 14 MeV neutrons via elastic scattering because of the non-trivial contribution of gamma rays. However, an inelastic collision inside the moderator producing a gamma ray does not necessarily produce an error in the total integrated energy deposition, if that gamma ray is also absorbed in the moderator. The amount of energy lost from the calorimeter by escaping gamma rays can be estimated in

the following manner. The inelastic scatter cross-section to total cross-section ratio in the CH_2 mixture is 0.20 for 14 MeV neutrons, and the mean free path for gamma absorption is approximately 50 cm for 1 MeV gammas. It is assumed that approximately 50% of the energy lost by a neutron in an inelastic collision goes to gammas. The moderator will absorb about 70% of the gamma rays, assuming a uniform, isotropic source distribution, and thus approximately 3% of the energy associated with the inelastic collision will be lost from the calorimeter. This number will be slightly higher if one includes those neutrons that have elastically scattered but still retain an energy above the inelastic threshold (4.8 MeV than for carbon). However, it will still be less than 5%. For the purpose of these feasibility calculations, it is assumed that the amount of gamma ray energy lost via inelastic scatter is balanced by the amount gained via exothermic capture reactions, so the net error is zero. More sophisticated calculations can be done for final calibration.

The effects of neutrons scattering into the sides of the calorimeter, and of gammas produced outside of the calorimeter and (entering the calorimeter) must also be examined. This evaluation requires a two-dimensional model, which is described below.

IV. TWO DIMENSIONAL CALCULATIONS

The code DOT-3.5 (available from RSIC) was used for the two dimensional calculations. The model, a finite cylinder in r-z geometry with rotational symmetry, is shown in Figure 3. The source strength is again 2.4×10^{11} n/cm^3-sec in a 75 cm radius. A listing of the DOT input is given in Appendix C. (For general information, this model takes about 30 minutes C.P.U. time on an IBM 370/3033.)

Power deposition profiles along the central radial axis of the calorimeter calculated from this model are shown in Figure 4. At the front face, the total energy deposition, and the relative contributions of the source neutrons, fast neutrons, and the gammas are virtually identical to those calculated with the one dimensional model. In fact, the total energy deposition at the back of the calorimeter, and the position of occurrence of the order of magnitude drop (decade point) in total energy deposition are nearly identical in the one and two dimensional models. However, the relative contributions of the source component, fast neutrons, and gammas differ, as summarized in Table 3. Note that in the one dimensional model, the shift along the radial axis in the major contributor to energy deposition from source neutrons to fast neutrons to gammas reflects the moderation of the 14 MeV source neutrons to fast neutrons (still of high enough energy to contribute to energy deposition), and the ultimate thermalization and capture of the source neutrons, which is shown by the larger percentage contribution from gammas at the back of the calorimeter.

Table 3

Relative Contributions To Energy Deposition
1 - D vs 2 - D Calculations

	1 - D	2 - D	Radial Position (from the Front Face of the Calorimeter)
Source Neutrons	50%	50%	0 cm
Fast Neutrons	35%	35%	
Gammas	15%	15%	
Source Neutrons	15%	20%	
Fast Neutrons	50%	40%	40 cm (Decade drop in power deposition)
Gammas	35%	40%	
Source Neutrons	5%	5%	
Fast Neutrons	20%	55%	87 cm (Back of calorimeter)
Gammas	75%	40%	

The two dimensional model gives a different behavior, in that the relative contribution from fast neutrons steadily increases along the radial axis of the calorimeter, while that due to gammas remains constant. This demonstrates the effect of the streaming path (through air) that can not be represented in the one dimensional model. In the two dimensional model, neutrons are much more likely to reach points near the back of the calorimeter having only a few collisions. Hence, the degree of thermalization is less, as shown by the greater contribution from the fast neutrons.

V. EFFECT OF THE TF COILS

The DOT model described in the previous section was modified by replacing the zones containing the TF coil and case with air to determine the effect of the TF coils on power deposition profiles in the calorimeter. It would be expected that the greatest effect would be seen along the edge of the calorimeter.

A comparison of power deposition radial profiles (total and the contribution from source neutrons alone) along the edge of the calorimeter with and without the TF coils present is given in Figure 5. It is seen that the TF coils have very little effect on energy deposition until a radius of about 156 cm is reached, which is approximately the radius of the front edge of the TF coil case. From that point backward, the coils provide a strong attenuation of neutron flux, and hence, energy deposition rates. Because there is no appreciable influence at radii where the TF coils do not block direct paths from the source to the calorimeter, it can be concluded that the backscattering of neutrons off the coils into the calorimeter is insignificant. The effect of the coils is simply that of a strong attenuating material placed in the line of sight from the source, which in fact is

beneficial as it helps to decrease the contribution to energy deposition from neutrons entering the sides of the calorimeter. The question of additional gammas produced in the TF coils will be addressed in the next section. The decade point, which is about midway along the calorimeter, and the point of influence of the TF coils coincide approximately. Thus, it can be concluded that the TF coils will produce less than a 10% perturbation on the total energy deposition even at the edge of the calorimeter.

The effect of the TF coils on the radial profiles of energy deposition along the central axis of the calorimeter is shown in Figure 6. The above conclusions are valid, and additionally, it is seen that the effect of the TF coils on energy deposition along the central radial axis is less than along the edge of the calorimeter.

VI. EFFECT OF EXTERNAL GAMMA RAYS

The effect of non-elastic neutron collisions outside the calorimeter can be determined by examining the energy deposition due to gammas alone. The radial profiles of energy deposition due to gammas along the edge and along the central axis of the calorimeter are shown in Figures 7 and 8, respectively. The effect of the lead shield is also demonstrated in these figures. First, it is clear that the lead shield does decrease the contribution from gammas, and the effect is more pronounced at the edge than at the center. However, the gamma energy deposition at the edge of the calorimeter decreases more rapidly at points beyond the line of sight point of the TF coils, both with and without the lead shield. This indicates that the TF coils significantly attenuate neutrons without producing an extraordinary source of intense gamma rays (i.e., the gamma contributions remain proportionate to the neutron contributions).

However, gammas produced outside the calorimeter must have a non-trivial effect, because of the difference in the profiles with and without the lead shield. This effect is seen along the central axis of the calorimeter as well (although it is smaller than along the edge).

The three major contributors to gamma rays are the stainless steel vacuum vessel, the TF coils, and the moderator itself. To determine the contribution from the vacuum vessel, the DOT model shown in Figure 3 was modified by replacing the zone of SS-304 with air. The power deposition profiles along the edge and along the central axis due to gammas with this modification are shown in Figures 9 and 10. Comparing these figures with Figures 7 and 8, it can be inferred that gammas produced in the stainless steel vacuum vessel contribute about 30% to all central axis gamma energy deposition at the front face, but nearly zero at the decade point and beyond. The percentage contribution is slightly greater along the edge of the calorimeter, but again at the decade point and beyond it is insignificant.

Also noted is the fact that the gamma energy deposition along the central axis is actually greater than along the edge, both with and without the stainless steel vacuum vessel. Without the lead shield, this difference is smaller, indicating that the shield protects the edge from external gammas, but the dominant contribution at the center is due to gammas produced in the moderator itself. At the front face, at least 30% of the gamma energy deposition comes from the vacuum vessel. However, the contribution from all gammas is only 15% of the total energy deposition at the front face. Since the gammas produced in the vacuum vessel do not have an effect beyond the decade point, the overall effect of the vacuum vessel must be less than 5% of the total integrated energy deposition.

VII. EFFECT OF ADDITIONAL COMPONENTS

It would be virtually impossible to model in detail the components (e.g., piping, structural, diagnostics, etc.) that will occupy part of the available space modelled as air in Figure 3. However, it is useful to get some idea of the potential effects of such components. To attempt to model the environment the air space of Figure 3 was uniformly filled with the stainless steel of the vacuum vessel, at half its density. Power deposition profiles along the edge and along the center are given in Figures 11 and 12, respectively. As would be expected, the effects along the edge are quite pronounced with the effect of the line of sight (from the source) attenuation very definite. The perturbation due to the TF coil is virtually removed when the void is filled with this material. However, when Figure 12 is examined, it is clear that the effect of this material is quite small along the central axis of the calorimeter, particularly at radii less than the decade point. These curves, in conjunction with Figures 5 and 6, indicate that the central region of the calorimeter up to the decade point is effectively isolated neutronically from components/materials to the sides of the calorimeter (the exception being the vacuum vessel at the front face).

VIII. CORRELATION OF POWER DEPOSITION PROFILES TO INCIDENT 14 MeV FLUX

Ultimately, it is desired to relate measured temperature profiles to the incident 14 MeV neutron flux. If it is assumed that the calorimeter is adiabatic, the temperature profile will be proportional to the power deposition profile. The procedure for determining the incident 14 MeV flux from such a power deposition profile is demonstrated below.

Based on the results given in previous sections, it is assumed that the central axis is well isolated from outside effects, and that with the lead

shield in place, the only source of error in energy deposition into the calorimeter will be those gammas produced in the vacuum vessel, (which should be less than 5%). Thus, it is assumed that the energy deposition due to these gammas must be subtracted from the total energy deposition.

The total energy deposition profile shown in Figure 5 was integrated along the extent of the axis of the calorimeter, yielding an integrated power deposition of 2.10×10^6 rads-cm/sec. The amount of integrated power deposited due to gammas produced in the vacuum vessel is obtained by subtracting the profile shown in Figure 10 from that shown in Figure 8, and integrating along the length of the calorimeter. This yields 7.2×10^4 rads-cm/sec. Subtracting this from the total integrated power deposition yields 2.03×10^6 rads-cm/sec, or using $\rho =$. gr/cm^3 and the appropriate conversions, an energy flux of 1.2×10^8 ergs/cm^2-sec. For 14-MeV neutrons, this corresponds to an incident flux of 5.43×10^{12} neutrons/cm^2-sec. The actual flux predicted in the DOT model is 5.36×10^{12} neutrons/cm^2-sec. Thus, it appears that if one can accurately relate measured temperature profiles to power deposition profiles, then one can infer the 14-MeV incident flux to high accuracy, with the aid of relatively simple neutronics calculations. Once the 14 MeV flux incident on the face of the calorimeter is known, it is a straightforward exercise to infer the fusion neutron source strength by accounting for geometrical factors and attenuation through the vacuum vessel.

IX. CONCLUSIONS

1. A one-dimensional neutronics model is adequate for calculating the energy deposition along the central axis of the calorimeter up to the decade point; beyond, there will be errors because of non-representation of streaming to points away from the front face.

However,in integrating the total power deposition along the central axis, the overall integrated error inherent to the one-dimensional model is less than 10%.

2. The TF coils provide additional attenuation of neutrons entering the sides of the calorimeter, and thus increase the isolation of the central axis. Backscattering off the coils, and extra gamma rays produced in the coils are not significant additions to the total power deposition along the central axis. Other TFTR components immediately outside the calorimeter will provide extra attenuation of neutrons entering the sides in the same manner as the TF coils.

3. External gamma rays deposit significant amounts of energy in the calorimeter, making a lead shield required around the sides With the lead shield, the central axis is isolated from all but gammas produced in the vacuum vessel. More calculations can be performed to determine more precisely the effect of inelastic scattering and exothermic capture reactions within the moderator. However, it is estimated that the maximum error introduced by neglecting gammas produced in the vacuum vessel is 5%, by neglecting inelastic collisions in the moderator, 5%, and by neglecting exothermic capture gammas in the moderator,5%.

4. Assuming no errors in the measurement of temperature changes, the fusion neutron fluence incident on the calorimeter can be determined simply from the measured temperature profile along the central axis to an accuracy of better than ±10%. A more precise determination requires the use of neutronics calculations for estimation of the perturbing effects.

ACKNOWLEDGMENTS

The author wishes to thank Dr. D. L. Jassby of Princeton Plasma Physics Laboratory for suggesting this investigation and for many useful discussions.

The cross-section set used in these calculations was collapsed by L. P. Ku of Princeton Plasma Phyics Laboratory, and the 2-D DOT model is a modification of his TF Coil Model.

This work was supported by the United States Department of Energy, Office of Fusion Energy, Contract No. DE-AC02-76-CHO-3073.

REFERENCES

1. "Tokamak Fusion Test Reactor Final Design Report", Princeton Plasma Physics Laboratory, Report PPPL-1475 (August 1978).

2. "An Absolute Fusion Energy Monitor for the TFTR", D. L. Jassby, Third Topical Conf. on High Temperature Plasma Diagnostic, Bull. Am. Phys. Soc., 25 (1980) p. 701.

3. "A Fusion Energy Calorimeter for the Tokamak Fusion Test Reactor", D. L. Jassby and G. R. Imel, to be presented at the Fourth ANS Topical Meeting on the Technology of Controlled Nuclear Fusion, King of Prussia, PA, October 14-17, 1980.

APPENDIX A

Third APS Topical Conference on

High Temperature Plasma Diagnostics

Los Angeles, California, 17 to 19 March 1980

Bull. Amer. Phys. Soc. 25 (1980) 701

An Absolute Fusion Energy Monitor for the TFTR*

D. L. JASSBY, Princeton Plasma Physics Lab.-- In a pulsed fusion device such as the TFTR, the fusion-neutron production per pulse can be measured absolutely by the temperature rise ΔT in an adiabatic neutron-absorption calorimeter located just outside the vacuum vessel. From the points of view of sensitivity [$\Delta T \propto$ (density x spec.heat x absorp. length)$^{-1}$], and feasibility of implementation and modification, the most promising working medium for the calorimeter is a type of lubricating oil. The depth of the working medium for at least 90% neutron energy absorption is about 30 cm. $Q \doteq 1$ conditions in the TFTR should result in $\Delta T \approx 0.4°C$ per 1-s pulse (14-MeV fluence = 5×10^{12} n/cm^2). This ΔT is at least 2 orders of magnitude larger than the threshold for detection with thermistors employed in a resistance-measuring bridge. Thus even modest fusion performance ($Q \gtrsim 0.1$) can be evaluated accurately. Design of the geometric configuration of the absorbing medium and of the calorimeter environs has been carried out to minimize the effects of scattered neutrons and gamma-rays that enter the sides of the calorimeter.

*Work supported by U.S.D.O.E. Contract EY-76-C-02-3073.

A-2

Submitted to the Fourth ANS Topical Meeting on the Technology of Controlled Nuclear Fusion, King of Prussia, Penn., Oct. 14-17, 1980

A FUSION ENERGY CALORIMETER FOR THE TOKAMAK FUSION TEST REACTOR

D. L. Jassby and G. R. Imel*
Plasma Physics Laboratory, Princeton University
Princeton, N. J. 08544

Configuration. In a pulsed fusion reactor such as the TFTR (Tokamak Fusion Test Reactor[1]), the fusion energy production per pulse can be monitored by means of an adiabatic total neutron-absorption calorimeter located just outside the vacuum vessel wall, as indicated in Fig. 1. In each fusion pulse the neutron moderating region of the calorimeter will experience a temperature rise proportional to the absorbed fusion-derived energy. The calorimeter presently being designed for the TFTR is large enough to serve as a simple blanket module, and in fact represents a primitive first step toward a power-producing blanket.

Choice of Neutron Moderator. The preferred moderator has (i) low density, (ii) low specific heat, (iii) high cross section for elastic neutron moderation, and (iv) low heat conduction. These requirements imply that moderators with low-Z atom constituents are preferable. Liquid hydrogen has the highest sensitivity, but it would require an elaborate cryogenic facility, and would always present the danger of explosion. From the points of view of sensitivity, safety, ease of handling, and cost, certain oils that are pure hydrocarbons appear to be the most suitable liquid moderating media, with polyethylene (CH_2) as a candidate solid medium. These materials have up to 2.5 times the sensitivity of water.

Power Deposition. ANISN calculations of the radial profiles of energy deposition in CH_2 are shown in Figure 2. The input source spectrum and intensity were calculated by the DOT code, and include ambient gammas and neutrons scattered from adjacent TFTR components. Almost half the incident neutron energy deposited near the front face is due to sub-14 MeV neutrons. About 10% of the total energy deposited at the front face is gamma radiation. Other ANISN calculations show that gammas produced in the CH_2 account for only 60% of the total gamma energy deposition (including ambient TFTR gammas) along the major radial axis. The gammas are the dominant component of the total energy deposition at locations 25 cm or more from the front face. However, the total energy deposition density at this point and beyond is down by an order of magnitude from the value near the front face.

Except at the front face, ambient gamma rays from the TFTR structure can be stopped by approximately 6 cm of lead shielding.

Maximizing the lateral extent of the moderator appears to be the optimal method for ensuring adequate isolation of the central region from boundary effects. The half-width of the moderator ($\simeq$ 40 cm in each direction) is sufficiently large so that scattered low energy neutrons entering the sides, either by reflection of moderator neutrons or from the TFTR ambient, are found to have 10% or less effect on the energy deposition along the major radial axis.

Sensitivity. Temperature increases ΔT will be measured by thermopiles and platinum-resistance thermometers distributed along the major radial axis and at other positions, as indicated in Fig. 1. Using one of the more sensitive hydrocarbons as the moderating medium, D-T operation in the TFTR with fusion power amplification $Q \simeq 1$ for 0.5 s will give $\Delta T \geq 0.2^{0}$ C near the front face, which would produce an easily measured 0.1% change in resistance of a resistance thermometer. With pulses of several seconds length, a well-insulated calorimeter could undergo a ΔT of several tens of degrees during a multi-hour run (duty factor ~ 0.01).

The calorimeter instrumentation will provide experimental data on power deposition profiles. In order to obtain an accurate evaluation of the total incident energy fluence, ΔT must be integrated along the major radial axis. The deomonstration of the ability to correlate the power deposition in a single module to the total fusion power production, and to calculated power deposition profiles (Fig. 2), will provide valuable information for the design of experimental power modules for next-generation tokamaks.

Acknowledgement. This work was supported by the U.S. Dept. of Energy, Office of Fusion Energy, under Contract No. EY-76-C-02-3073.

Reference

1. "Tokamak Fusion Test Reactor Final Design Report", Princeton Plasma Physics Lab. Report PPPL-1475 (August 1978).

---

*On leave from EG&G Idaho, Inc., Idaho Falls, ID 83415.

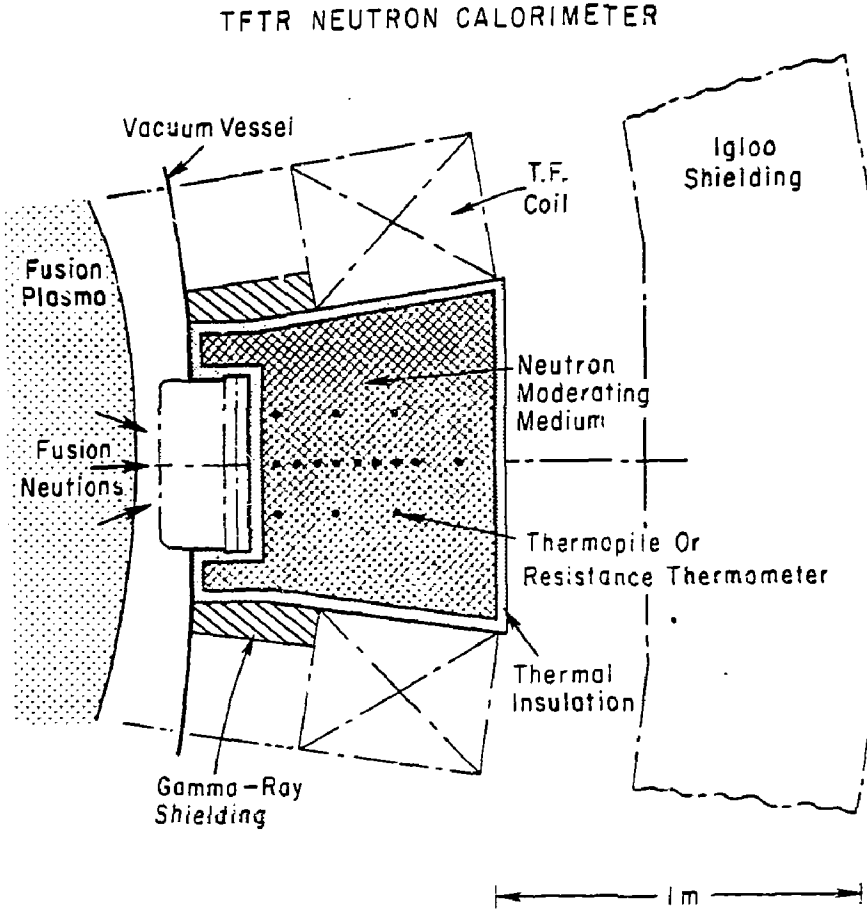

Figure 1. Plan view showing location of the neutron calorimeter with respect to the TFTR plasma.

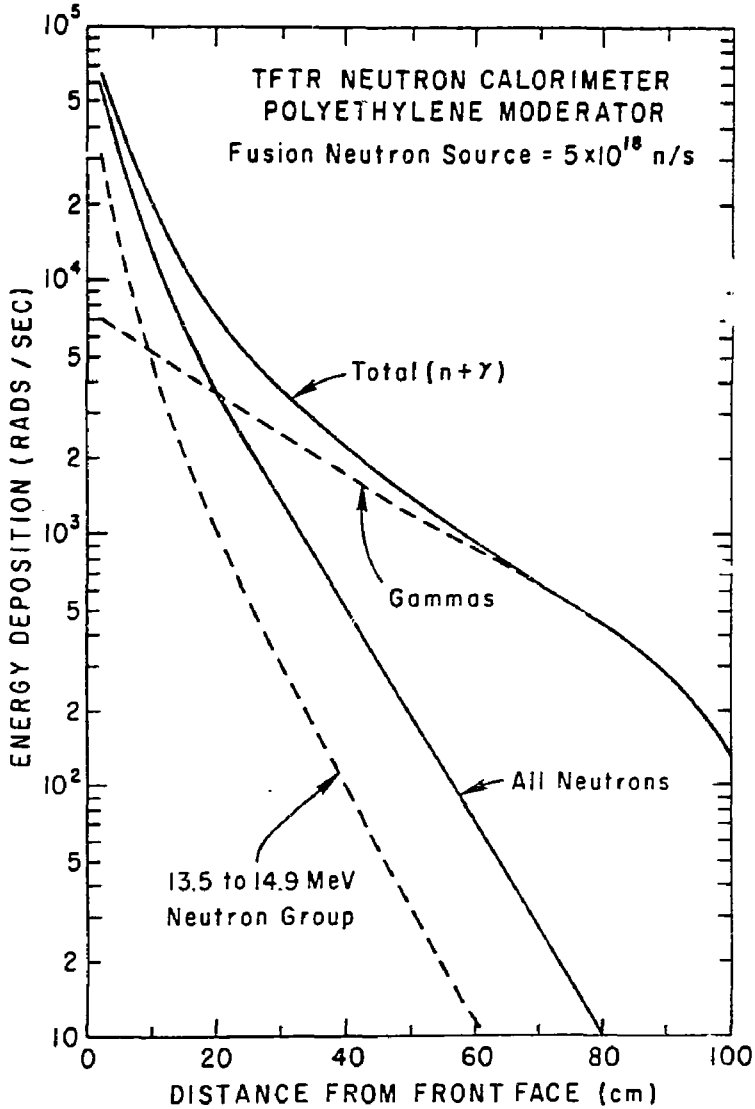

Figure 2. ANISN calculations of energy deposition profiles in a polyethylene moderator.

APPENDIX B

```
FILE: ANISN     MODEL     A   PRINCETON UNIVERSITY TIME-SHARING SYSTEM


CALORIMETER CYLINDRICAL POLY
1C
1SS3 1 0 3 8 2 1 0 6 50 0 34 3 4 37 C C 3E 36 1 C 1 C C 100 4 1 C 0
1 1 C C 3 1 1 0
16** 2R0.0 1.0-4 6R0.C C.5 2.0-3 3R0.C T
17** 3R2.379+11 F0.C T
3** F0.0 T
1** F0.0
4** 2I0.0 1I 75.0 114.0 9I 115.3 155.0 157.0 160.0 9I 162.0
202.0 204.0 207.0 3I 209.C 250.C 253.2 258.2 263.2
268.2 274.2 279.2 284.2 289.2 4I 294.2 319.2
5** 7.042-2 7.752-2 8.547-2 9.434-2 .1C53 .122C .1471 .1786 .2174 .2703
.3333 .4 .5 .7143 1.25 2.5 6.333 50.C 555.6 6667. 8.3+4 8.3+5 4.762+6
.07692 .1 .133 .154 .182 .222 .286 .4 .667 1.667 10.C
6** C.0 0.0604938 0.0453704 3N2
C.C C.0453704 0.0462962 0.0453704 1N3
0.C 4R0.0453704
0.0 2R0.0604938
7** -.9759 -.9511897 -.7867958 -.5773503 -.2182179 1M4
-.9164965 -.7867958 -.5773503 -.2182179 1M3
-.6172134 -.5773503 -.2182179 1M2
-.3086067 -.2182179 +.2182179
8** 5R1 2 23R3 4 7R5 13R6
9** 9 1 33 29 5 21
1953 F3
21** F1.0 I
  I            I
```

APPENDIX C

```
FILE: DOT       MODEL     A   PRINCETON UNIVERSITY TIME-SHARING SYSTEM


CALORIMETER DOT MODEL
5155  0  3  3  50  23  34  3  4  37  C
  0  0  36  1  48  1  1  0  1  1
  1  3  -15  3  0  0  450  3B0  0  1  5B0  1  4H0  5B0
  2  1  4  0  0  0  0  0  0  31  0
6255  10  12  11  2  3  13  4  20  1  21  0  90  0  0
63**  0.0  1.0-2  1.0-2  60.0  F 0.0
T
 7*
 0 -27900- 5 0 -18343- 5 0 +18343- 5 0 -60441- 5 0 -52553- 5 0 -18343- 5
 0 +18343- 5 0 +52553- 5 0 -85078- 5 0 -79667- 5 0 -52553- 5 0 -18343- 5
 0 +18343- 5 0 +52553- 5 0 +79667- 5 0 -98303- 5 0 -96029- 5 0 -79667- 5
 0 -52553- 5 0 -18343- 5 0 +18343- 5 0 +52553- 5 0 +79667- 5 0 +96029- 5
 0 -27900- 5 0 -18343- 5 0 +18343- 5 0 -60441- 5 0 -52553- 5 0 -18343- 5
 0 +18343- 5 0 +52553- 5 0 -85078- 5 0 -79667- 5 0 -52553- 5 0 -18343- 5
 0 +18343- 5 0 +52553- 5 0 +79667- 5 0 -98303- 5 0 -96029- 5 0 -79667- 5
 0 -52553- 5 0 -18343- 5 0 +18343- 5 0 +52553- 5 0 +79667- 5 0 +96029- 5
 3R-96029- 5 5R-79667- 5 7R-52553- 5 9R-18343- 5 3R+96029- 5 5R+79667- 5
 7R+52553- 5 9R+18343- 5
  T
 6*
 0 +     0+ 0 2R+25307- 6 0 +     0+ 0 0 +35623- 6 2R+19972- 6 0 +35623- 6
 0 +     0+ 0 0 +35623- 6 0 +16254- 6 2R+26551- 6 0 +16254- 6 0 +35623- 6
 0 +     0+ 0 0 +25307- 6 0 +19972- 6 0 +26551- 6 2R+18840- 6 0 +26551- 6
 0 +19972- 6 0 +25307- 6 0 +     0+ 0 2R+25307- 6 0 +     0+ 0 0 +35623- 6
 2R+19972- 6 0 +35623- 6 0 +     0+ 0 0 +35623- 6 0 +16254- 6 2R+26551- 6
 0 +16254- 6 0 +35623- 6 0 +     0+ 0 0 +25307- 6 0 +19972- 6 0 +26551- 6
 2R+18840- 6 0 +26551- 6 0 +19972- 6 0 +25307- 6
  T
17**  3R2.37903+11  47R0.0  22Q50  T
17**  F 0.0  T
17**  F 0.0  T
17**  F 0.0  T
17**  F 0.0  T
17**  F 0.0  T
17**  F 0.0  T
17**  F 0.0  T
17**  F 0.0  T
17**  F 0.0  T
17**  F 0.0  T
17**  F 0.0  T
17**  F 0.0  T
17**  F 0.0  T
17**  F 0.0  T
17**  F 0.0  T
17**  F 0.0  T
17**  F 0.0  T
17**  F 0.0  T
17**  F 0.0  T
17**  F 0.0  T
17**  F 0.0  T
17**  F 0.0  T
17**  F 0.0  T
```

```
FILE: DOT       MODEL    A   PRINCETON UNIVERSITY TIME-SHARING SYSTEM


17**   E 0.0  T
17**   E 0.0  T
17**   E 0.0  T
17**   E 0.0  T
17**   E 0.0  T
17**   E 0.0  T
17**   E 0.0  T
17**   E 0.0  T
3** 34R  0.0  T
1**   E 0.0
5**   E 1.0
2**   -65.623   -50.00   -20.585  9I -17.725   17.727   8I 20.585
65.96
4**   2I 0.0   1I 75.0   114.0   9I 115.3   155.0   157.0   160.0   9I 162.0
202.0   204.0   207.0   3I 209.0   250.0   253.2   259.2   263.2
268.2   274.2   279.2   284.2   289.2   4I 294.2   319.2
8$$
5R1   2   31R3   13R6   10$0
5R1   2   10R3   3R4   10R4   3R4   5R3   13B6
5R1   2   10R3   3R4   10R5   3R4   5R3   13R6   9Q5C
5R1   2   10R3   3R4   10R4   3R4   5R3   13B6
5R1   2   24R7   7R3   13R6
5R1   2   23R8   7   7R3   13R6
7Q50
9$$   -9   -1   -5   -13   -17   -21   -29   -33
28$$   E 25
T
```

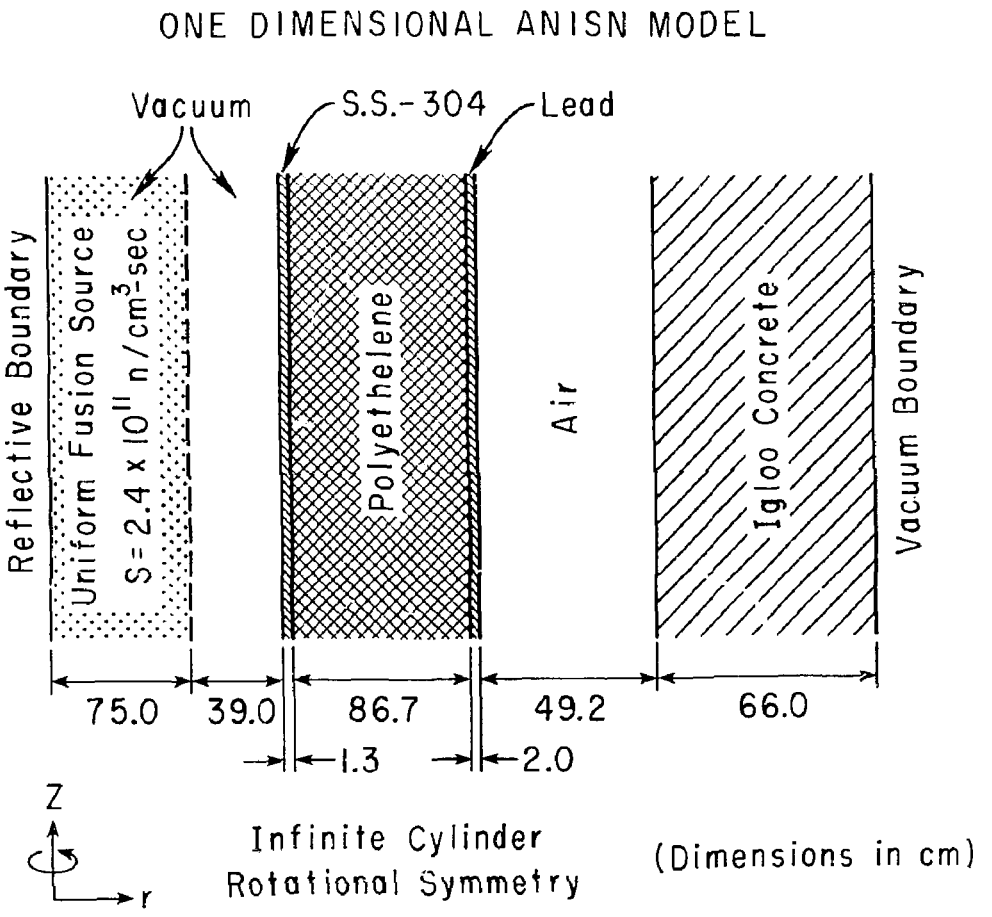

(PPPL-806306)

Fig. 1. One-dimensional neutron calorimeter model.

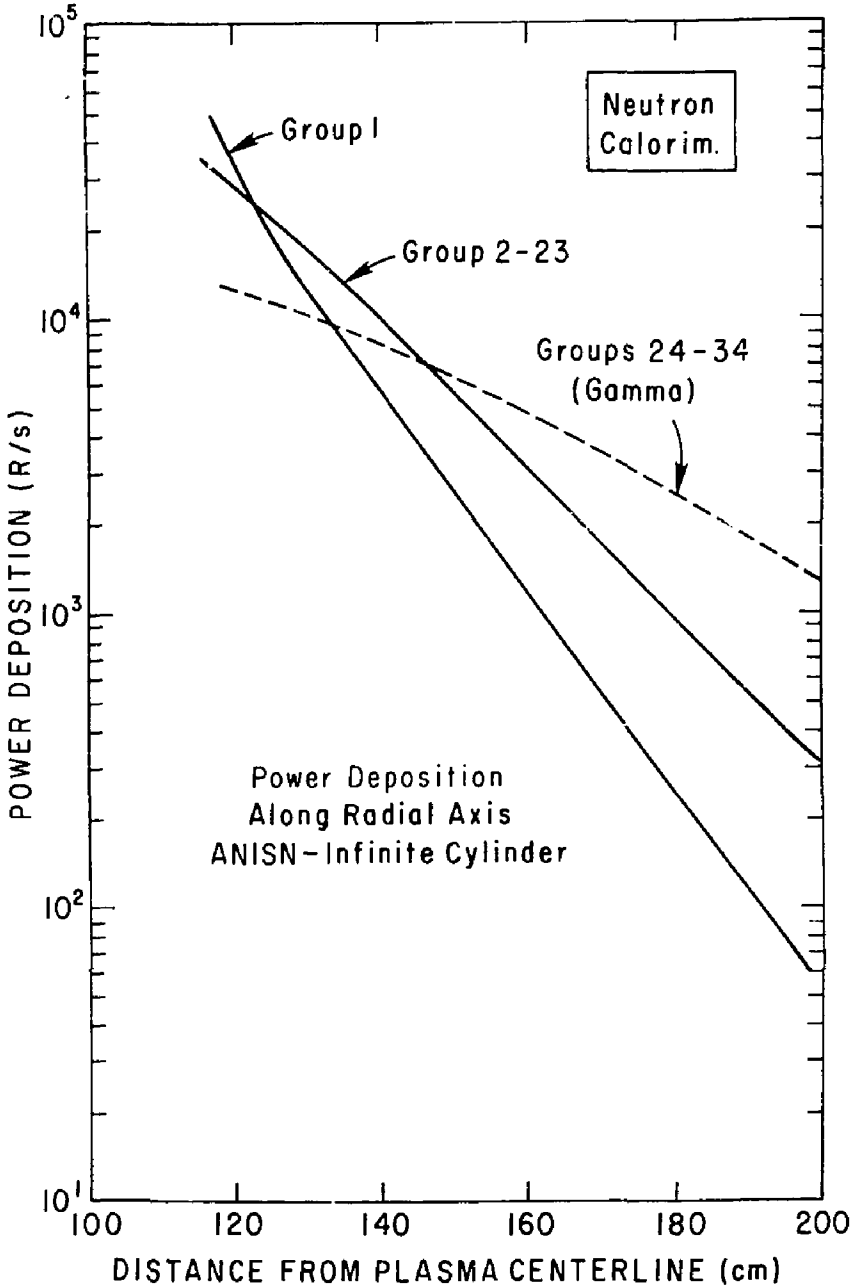

(PPPL-806309)

Fig. 2. Radial power deposition profiles along the central axis of the neutron calorimeter, calculated using the one-dimensional model.

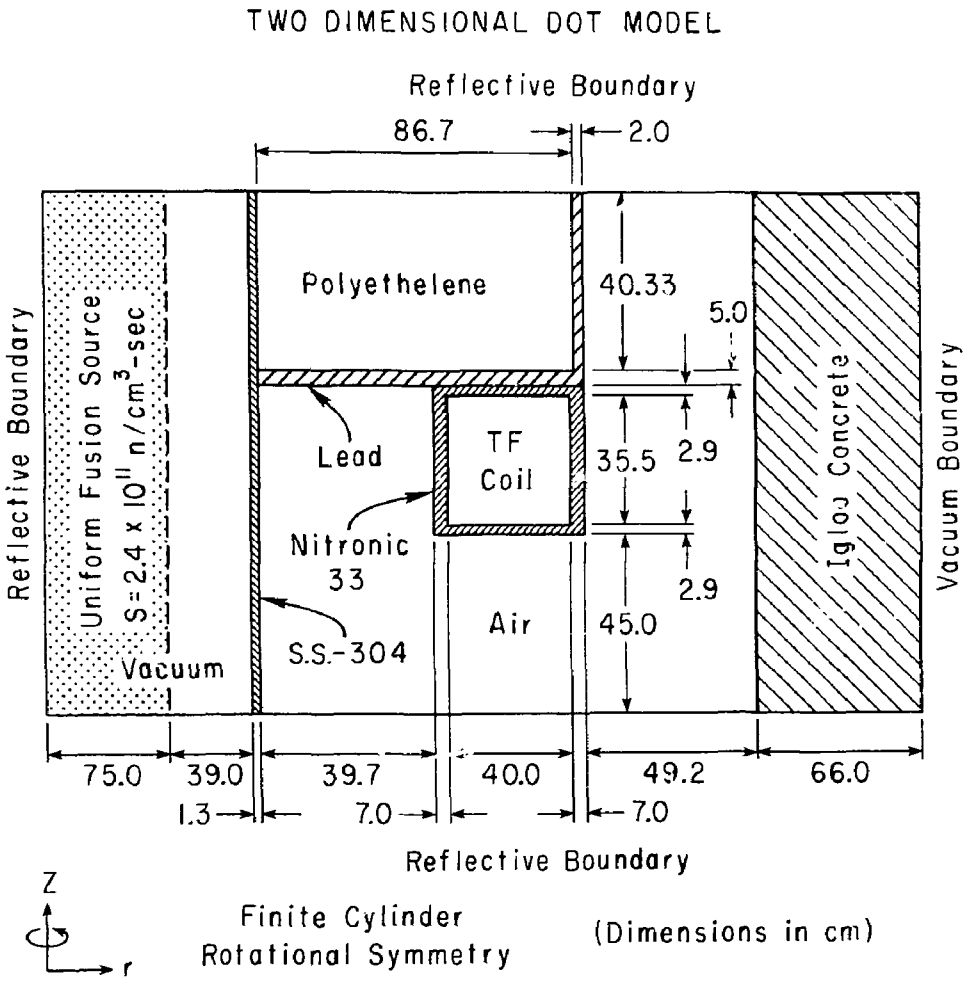

(PPPL-806301)

Fig. 3. Two-dimensional neutron calorimeter model.

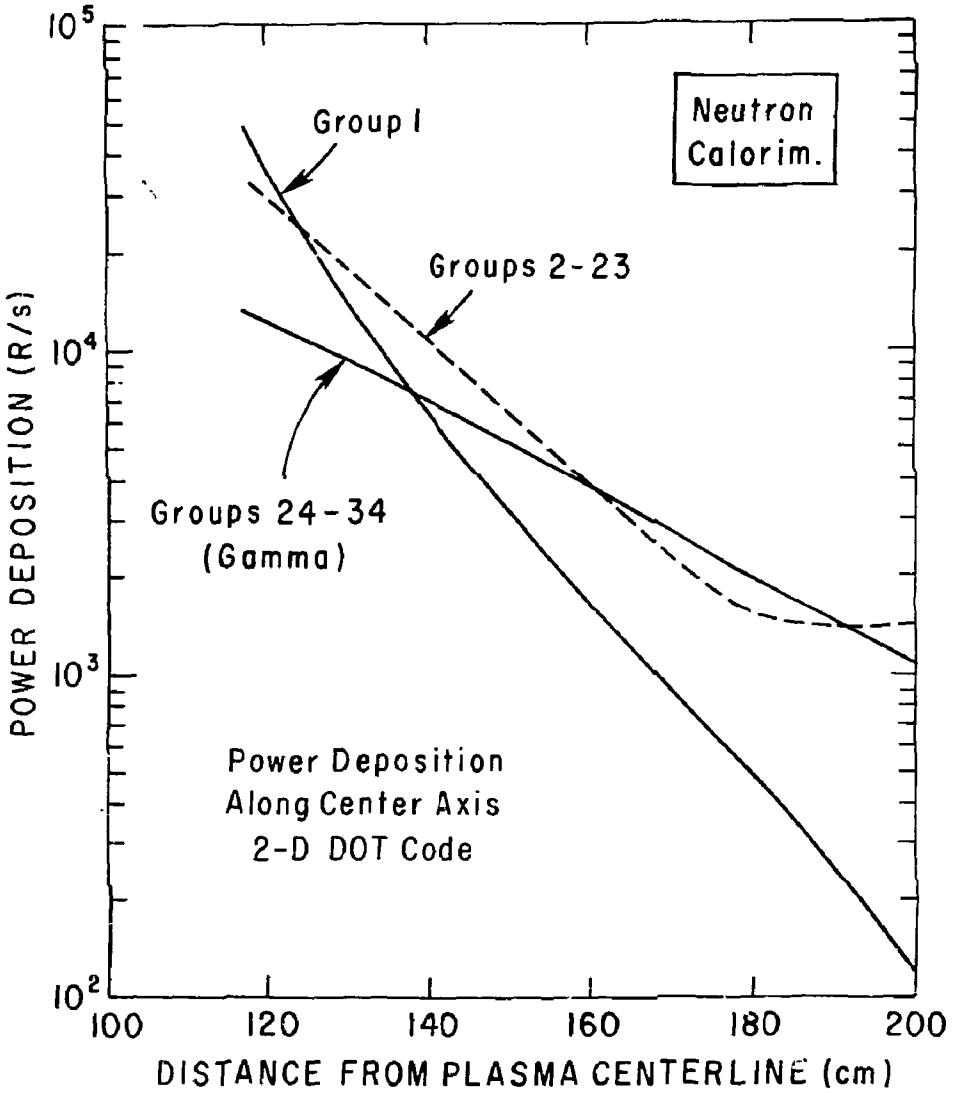

(PPPL-806308)

Fig. 4. Radial power deposition profiles along the central axis of the neutron calorimeter, calculated using the two-dimensional model.

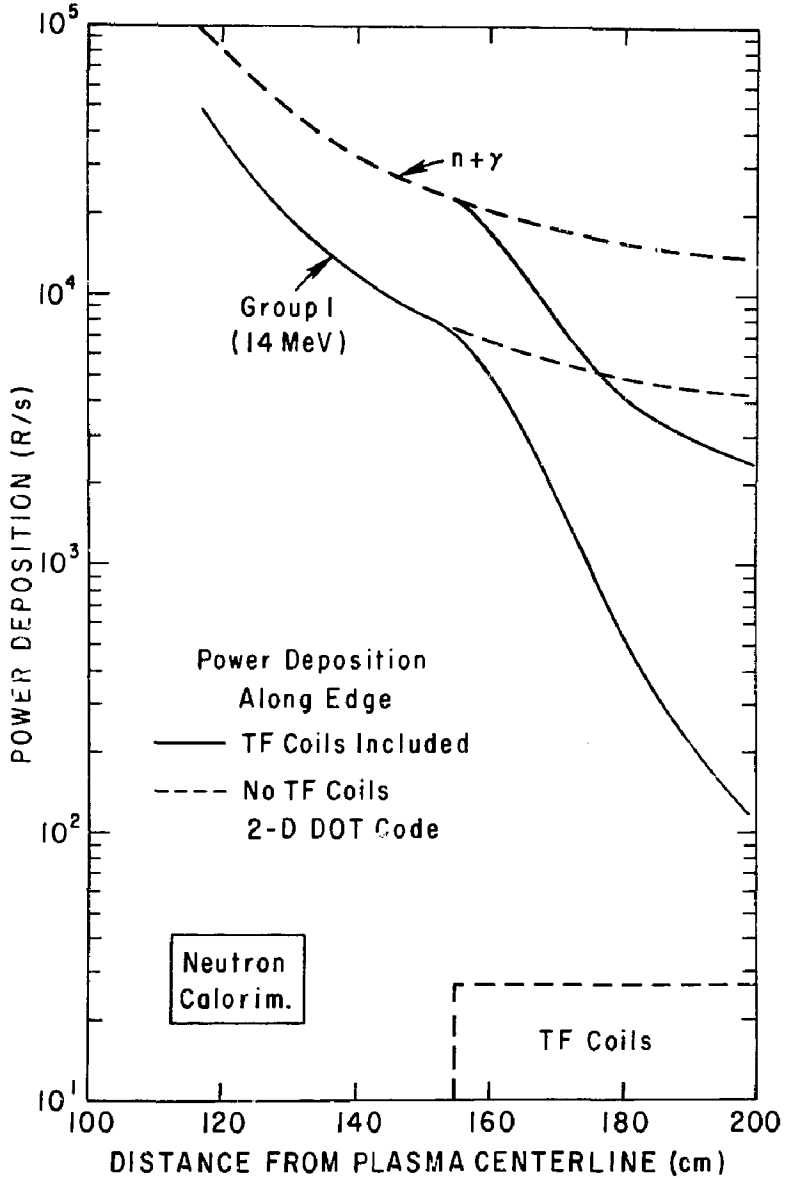

(PPPL-806304)

Fig. 5. Radial power deposition profiles along the edge of the neutron calorimeter showing the effect of the TF coils (2-D model).

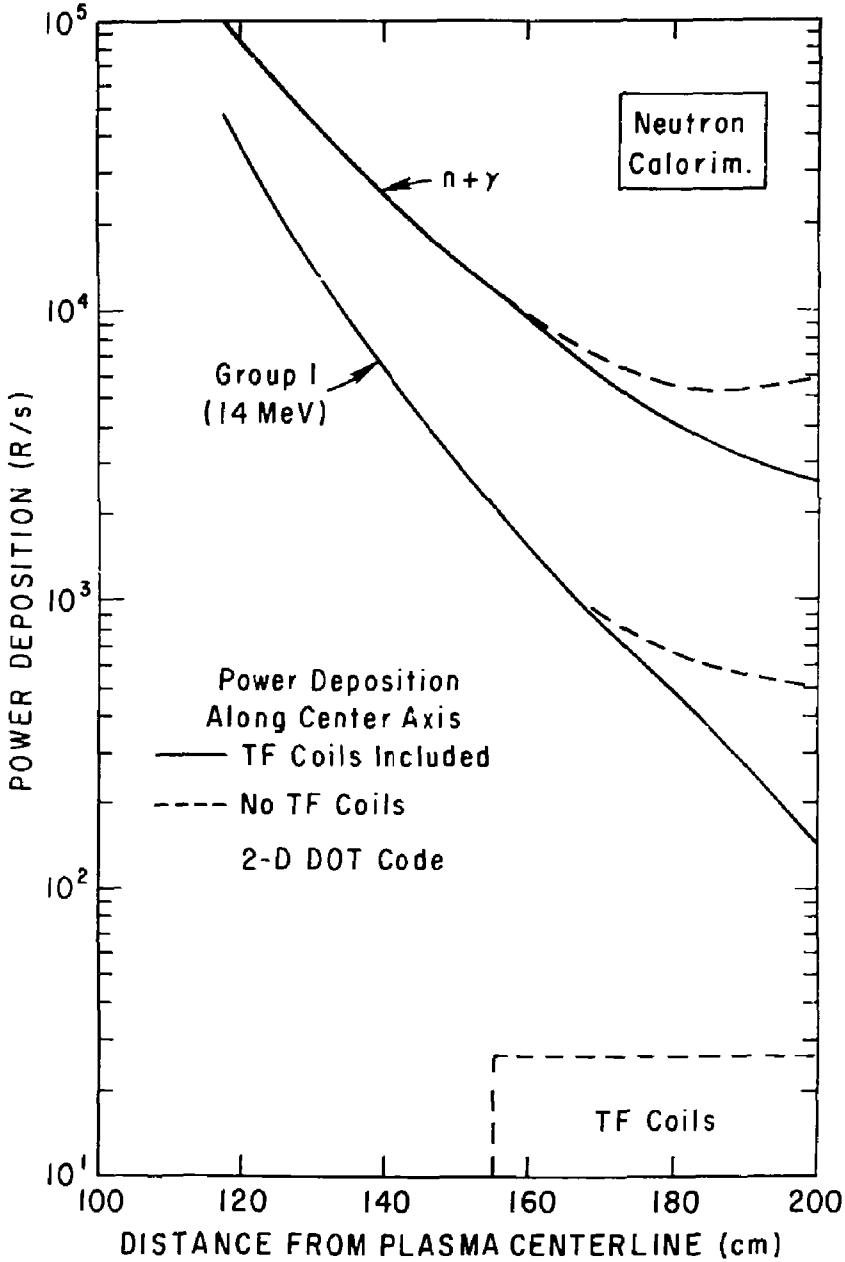

(PPPL-806305)

Fig. 6. Radial power deposition profiles along the central axis of the neutron calorimeter showing the effect of the TF coils (2-D model).

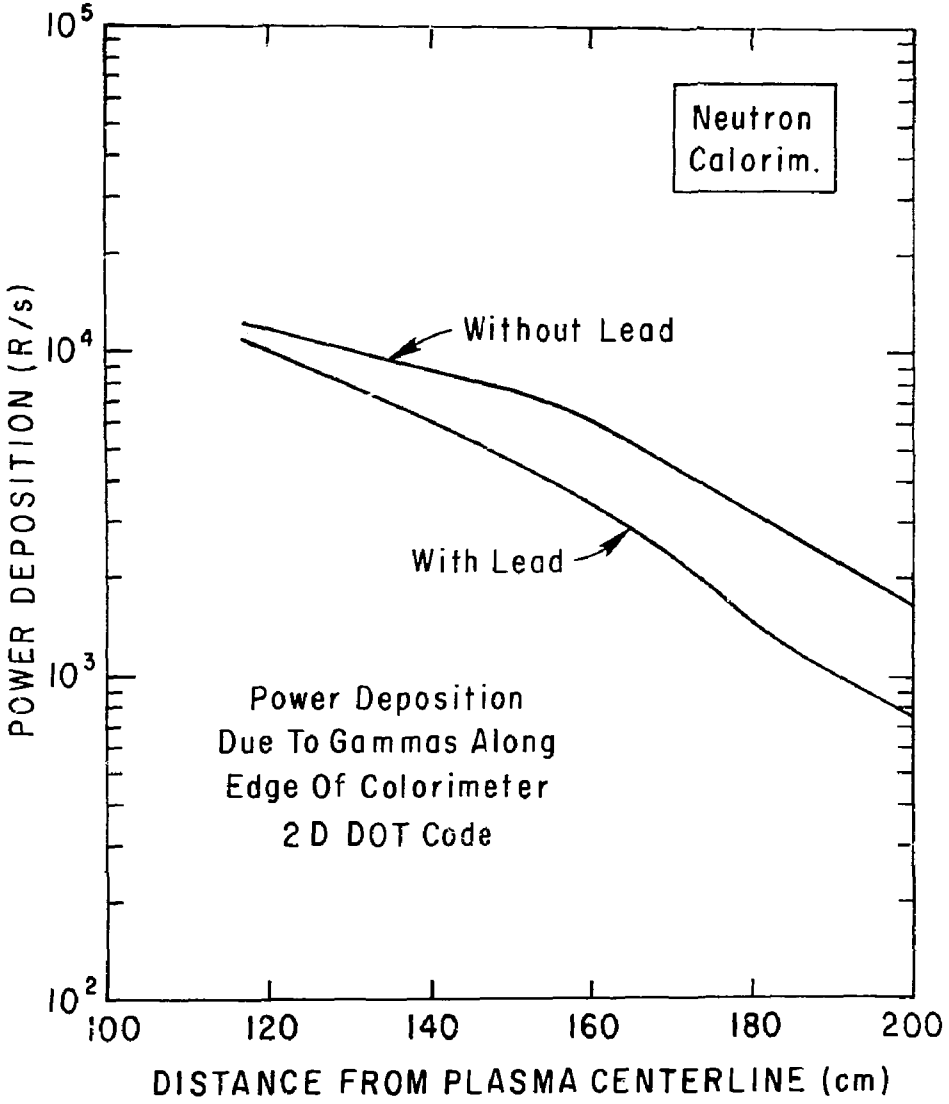

(PPPL-806310)

Fig. 7. Radial power deposition profiles of the gamma rays alone along the edge of the neutron calorimeter, showing the effect of the lead shield (2-D model).

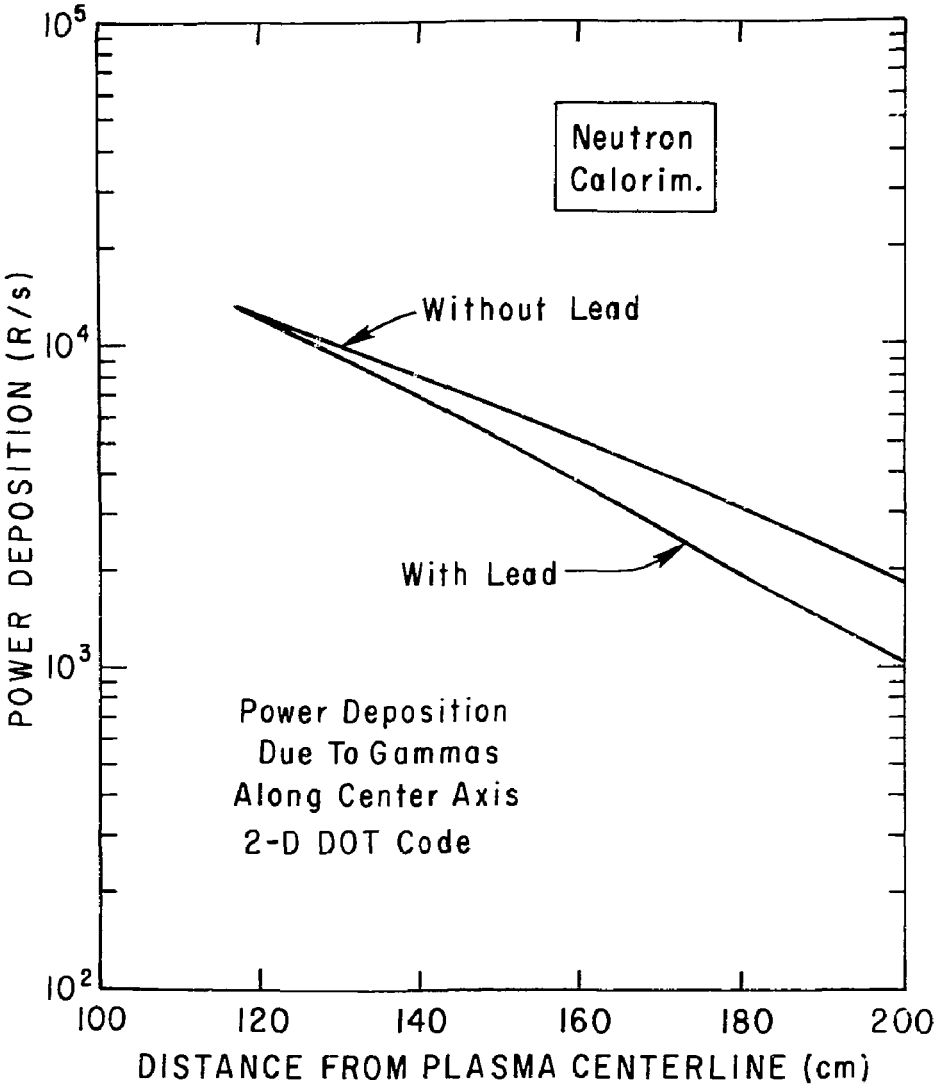

(PPPL-806302)

Fig. 8. Radial power deposition profiles of the gamma rays alone along the central axis of the neutron calorimeter, showing the effect of the lead shield (2-D model).

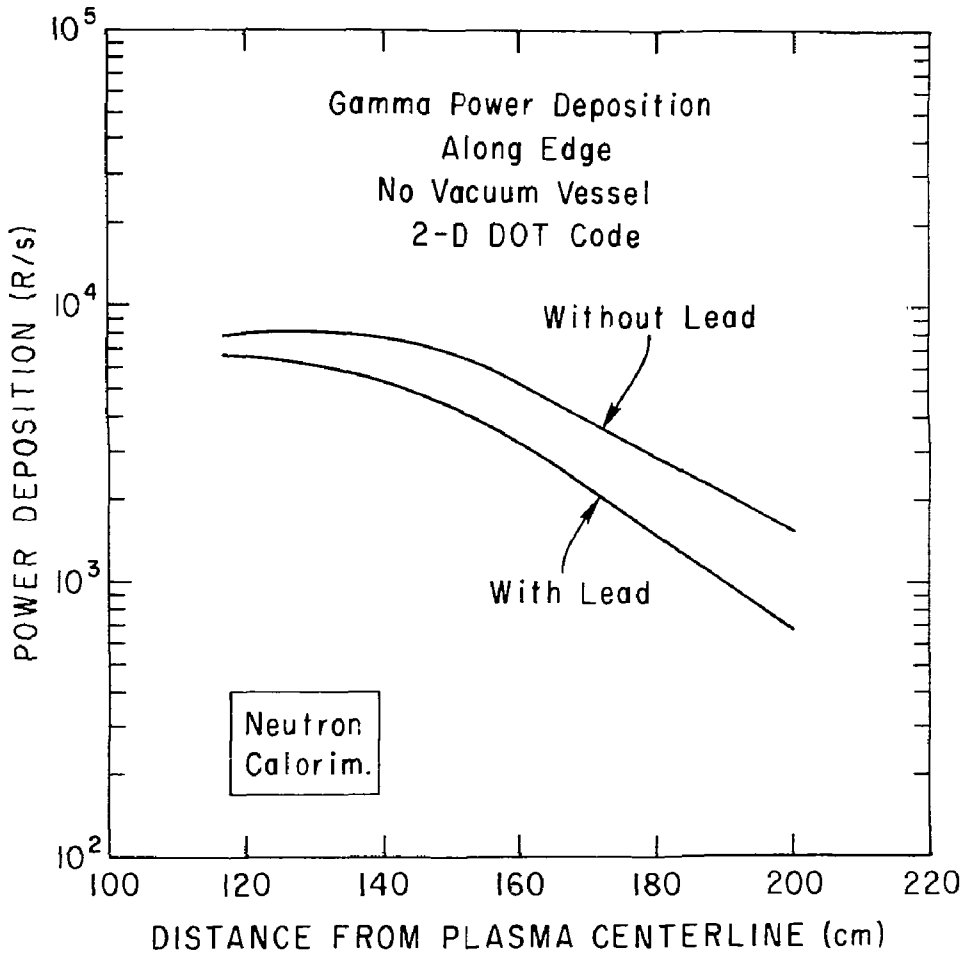

(PPPL-806307)

Fig. 9. Radial power deposition profiles of the gamma rays alone along the edge of the neutron calorimeter, without the vacuum vessel (2-D model).

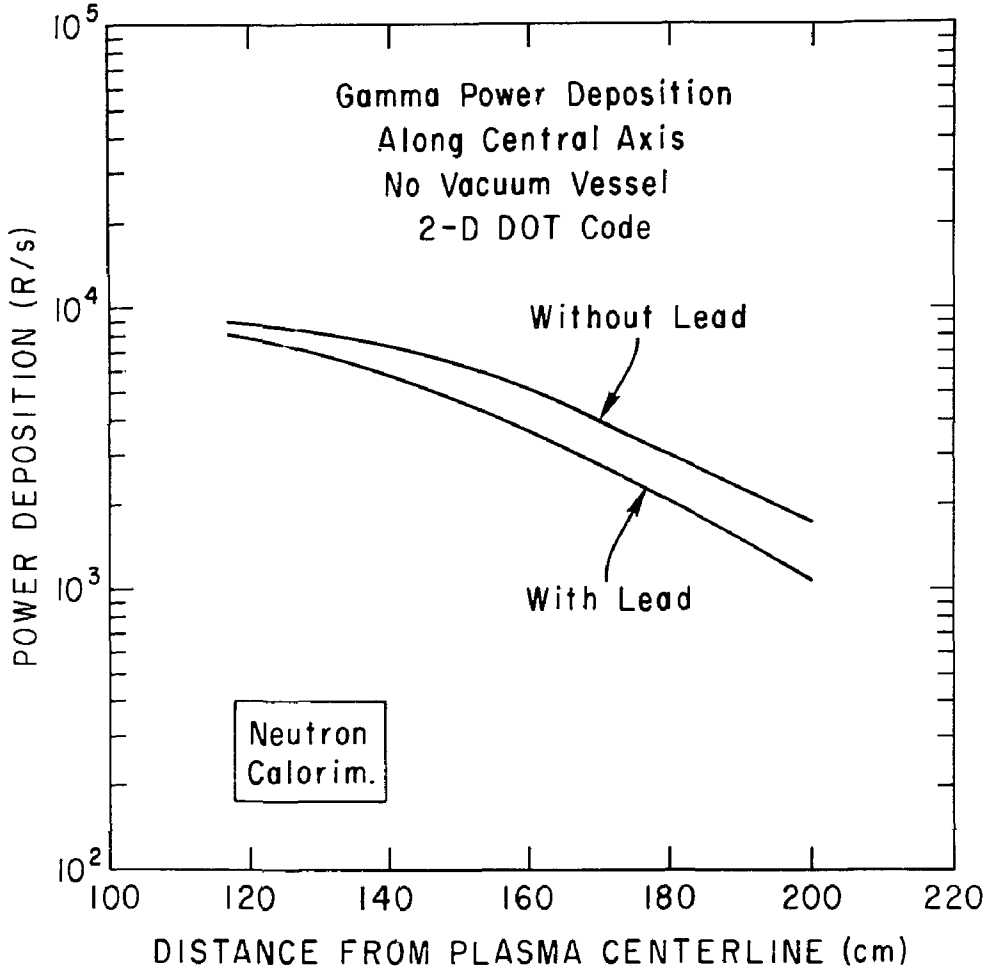

(PPPL-806303)

Fig. 10. Radial power deposition profiles of the gamma rays alone along the central axis of the neutron calorimeter, without the vacuum vessel (2-D model).

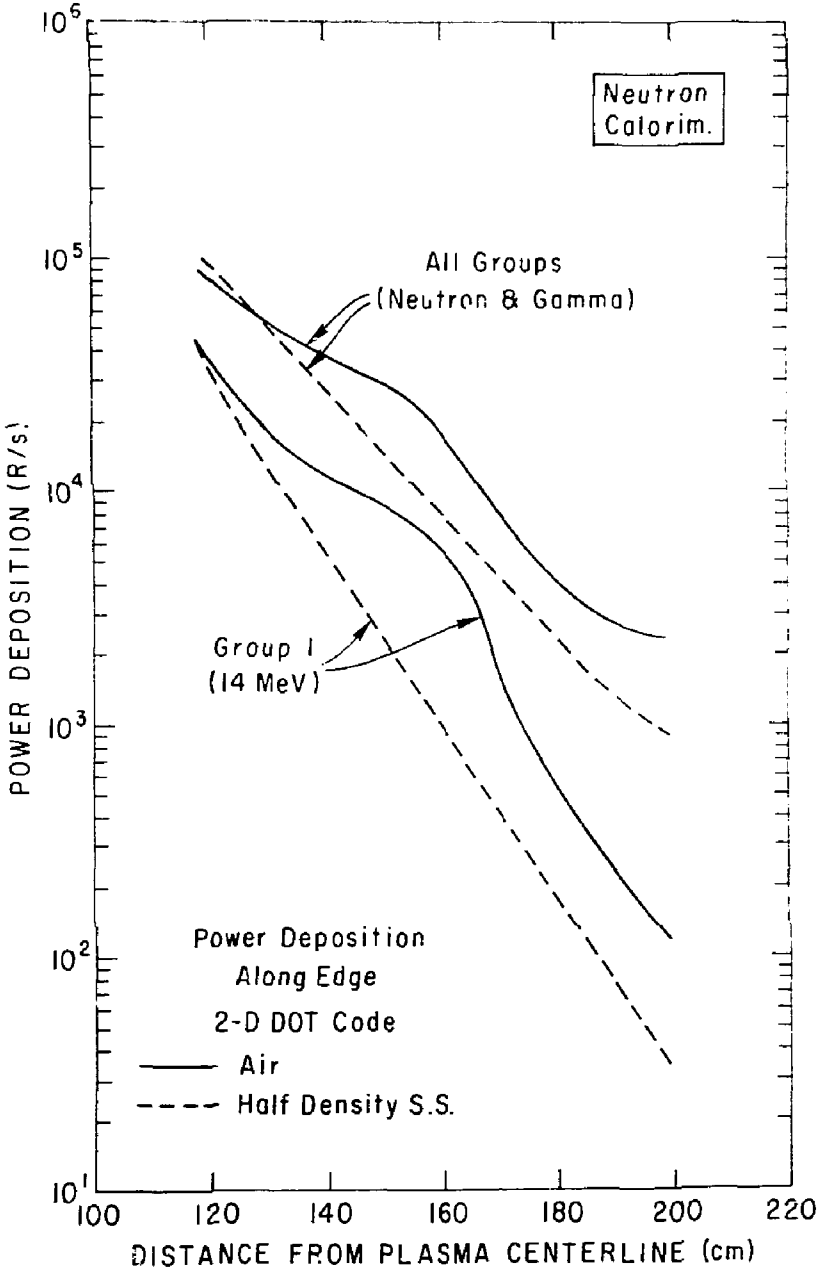

(PPPL-806300)

Fig. 11. Radial power deposition profiles along the edge of the neutron calorimeter, showing the effect of replacing the air streaming paths by low-density stainless steel (2-D model).

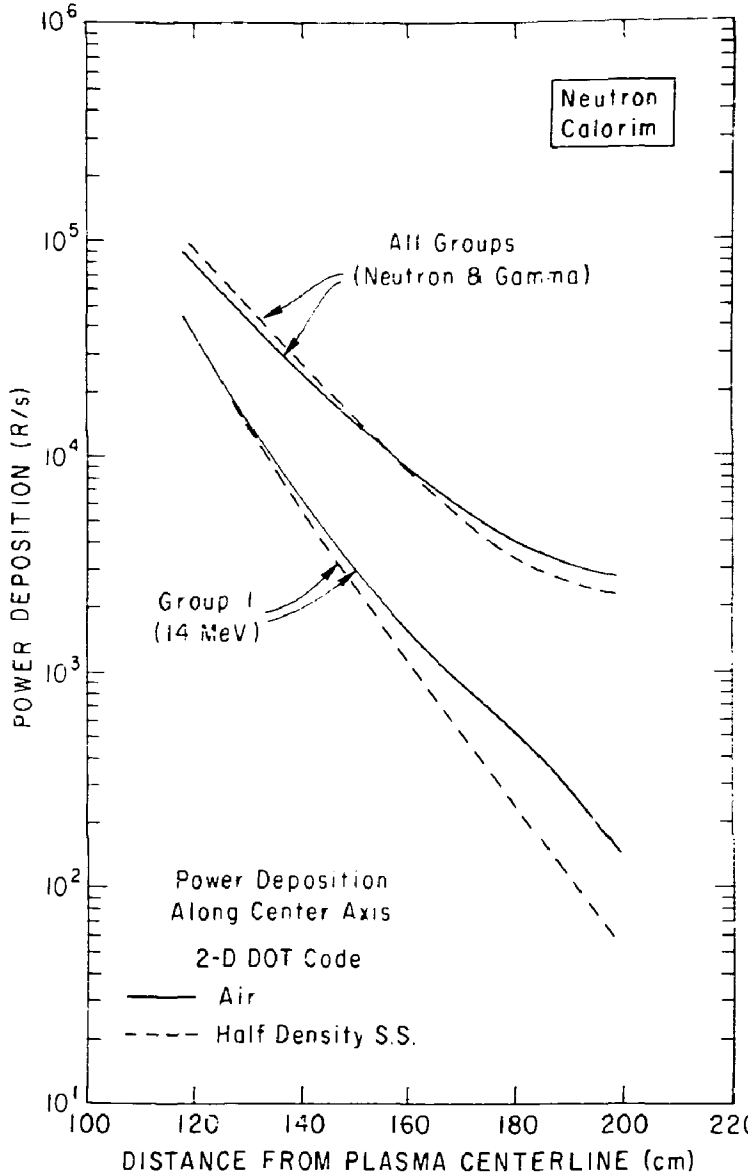

(PPPL-806299)

Fig. 12. Radial power deposition profiles along the central axis of the neutron calorimeter, showing the effect of replacing the air streaming paths by low-density stainless steel (2-D model).